Proc. Natl. Acad. Sci. USA
Vol. 89, pp. 10041–10045, November 1992
Biophysics

Extended x-ray absorption fine structure studies of a retrovirus: Equine infectious anemia virus cysteine arrays are coordinated to zinc

MARK R. CHANCE*, IRIT SAGI†, MICHAEL D. WIRT†, SUZANNE M. FRISBIE†, EVA SCHEURING†, EEFEI CHEN†, JULIAN W. BESS, JR.‡, LOUIS E. HENDERSON‡, LARRY O. ARTHUR‡, TERRI L. SOUTH§, GABRIELA PEREZ-ALVARADO§, AND MICHAEL F. SUMMERS§

*Department of Physiology and Biophysics, Albert Einstein College of Medicine, 1300 Morris Park Avenue, Bronx, NY 10461; †Department of Chemistry, Georgetown University, 37th and O Street, NW, Washington, DC 20057; ‡AIDS Vaccine Program, Program Resources Inc./Dyn Corp., National Cancer Institute–Frederick Cancer Research and Development Center, Frederick, MD 21701; and §Department of Chemistry and Biochemistry, University of Maryland at Baltimore, Baltimore, MD 21228

Communicated by Britton Chance, July 13, 1992 (received for review January 24, 1992)

ABSTRACT **Zinc finger arrays have been established as a critical structural feature of proteins involved in DNA recognition. Retroviral nucleocapsid proteins, which are involved in the binding of viral RNA, contain conserved cysteine-rich arrays that have been suggested to coordinate zinc. We provide metalloprotein structural data from an intact virus preparation that validate this hypothesis. Extended x-ray absorption fine structure (EXAFS) spectroscopy of well-characterized and active preparations of equine infectious anemia virus, compared with a peptide with known coordination and in combination with available biochemical and genetic data, defines a Cys_3His_1 coordination environment for zinc. The average of the Zn–S distances is 2.30(1) Å and that of the Zn–N distance (to histidine) is 2.01(3) Å.**

Zinc finger domains are known to be of great importance in a number of proteins that are involved in nucleic acid binding and transcriptional control. All known retroviral nucleocapsid (NC) proteins contain at least one sequence of the form Cys-Xaa_2-Cys-Xaa_4-His-Xaa_4-Cys, where Xaa represents various amino acids (1–4). Site-directed mutagenesis experiments involving point mutations of cysteine, histidine, and adjacent residues in the NC protein of murine leukemia virus indicate that the conserved arrays are intimately involved in retroviral RNA recognition, since these mutants give rise to virus particles with little or no detectible viral RNA (5, 6). Subsequent genetic experiments with human immunodeficiency virus type 1 (HIV-1) *gag* domains, which have two cysteine arrays rather than one, reveal that mutations in either Cys-His array reduce RNA packaging considerably, and infectivity even more drastically (7, 8).

Prior investigations have conclusively shown that synthetic peptides based on these conserved retroviral sequences bind Zn^{2+} tightly and stoichiometrically (also Co^{2+} and Cd^{2+}), and a wealth of spectroscopic evidence points to a three-cysteine one-histidine coordination for metals bound to these peptides (4, 9–11). The relevance of the peptides to virus function has been questioned, since the zinc content of avian myeloblastosis virus is reportedly insufficient to populate the cysteine arrays (12). However, more recent evidence clearly shows that the zinc content of HIV-1 and human T-cell leukemia virus type I (HTLV-I) is present in near stoichiometric amounts to the NC protein cysteine arrays (13). Thus, the potential importance of retroviral cysteine arrays and zinc to the physiological functions of nucleic acid binding and infectivity is illustrated by a wide range of investigations. We describe experiments that probe the zinc environment of concentrated preparations of equine infectious anemia virus (EIAV), a lentivirus (14, 15), using extended x-ray absorption fine structure (EXAFS) spectroscopy. Data obtained from analysis of virus was compared to that from a well-characterized 18-residue retroviral-type zinc finger peptide, based on sequences from HIV-1. This peptide has the sequence Val-Lys-Cys-Phe-Asn-Cys-Gly-Lys-Glu-Gly-His-Ile-Ala-Arg-Asn-Cys-Arg-Ala, and two-dimensional NMR studies of the zinc-reconstituted peptide show a discrete and ordered structure with the conserved Cys and His residues arranged in a tetrahedral configuration pointing toward the cation "hole" (16, 17). NMR studies of the ^{113}Cd adduct of this peptide clearly show the coordination of the cysteine array, so that this peptide has both a defined secondary structure and known ligation (9). Thus, the EXAFS signature of the peptide provides a touchstone for examining the zinc environment of retroviruses.

Our data demonstrate that the zinc present in EIAV is in an environment similar to that of the peptide with the expected Cys_3His_1 coordination. Although the zinc–ligand distances in the virus are 0.05 Å shorter and the virus site is more ordered, the extraordinary similarity of the two structures is remarkable. These results are of interest to drug designers and virologists, since it is vital to know the extent to which structures predicted from metal-containing peptide models are relevant to physiological virus preparations. Our results clearly demonstrate the relevance of zinc-peptide models in understanding zinc finger–nucleic acid interactions of retroviruses; further studies on longer peptides and purified NC proteins are of interest to identify other targets for antiviral drugs.

MATERIALS AND METHODS

Virus was grown as described previously (13) and was purified by two successive ultracentrifugations in sucrose density gradients in the presence of 1 mM EDTA. The first ultracentrifugation was continuous flow, the second was rate zonal. The virus fractions were pooled, diluted, pelleted, and resuspended at 1/5000th the volume of the original cell culture. Two EIAV preparations were analyzed for total protein (by the assay of Lowry *et al.*) and zinc (by atomic absorption after disruption in 1% SDS) (13). These fractions contained 13.7 and 10.7 μM zinc and protein at 1.75 and 1.65 mg/ml. Also, these amounts are consistent with zinc to

The publication costs of this article were defrayed in part by page charge payment. This article must therefore be hereby marked "*advertisement*" in accordance with 18 U.S.C. §1734 solely to indicate this fact.

Abbreviations: NC, nucleocapsid; HIV-1, human immunodeficiency virus type 1; HTLV-I, human T-cell leukemia virus type I; EIAV, equine infectious anemia virus; EXAFS, extended x-ray absorption fine structure; TPP, meso-tetraphenylporphyrin; FT, Fourier transformed.

protein ratios of other retroviruses measured previously, including HIV-1 and HTLV-I, where the zinc amounts have been shown to be near stoichiometric with the cysteine arrays (0.85 zinc atom per cysteine array). In addition, when HIV-1 and HTLV-I proteins were tested, only the NC protein bound zinc (13). The zinc present in these virus preparations is very tightly bound (as for the model peptides), since the zinc to capsid antigen ratio held relatively constant through three additional rate zonal ultracentrifugations in the presence of EDTA (13). To prepare samples for EXAFS the above two fractions were pooled and centrifuged at 100,000 × *g* for 45 min. The pellet was essentially a paste, and a portion of the EIAV was carefully scraped into a sample holder and frozen in liquid nitrogen. A portion of the paste was subjected to atomic absorption spectrometry and was found to have a zinc concentration of ≈1.5 mM. The zinc metallopeptide was prepared as described previously (16, 17) and was suspended in distilled water with a final concentration of 2.2 mM in zinc. The peptide concentration was 10% higher to ensure that all zinc atoms were coordinated.

Beamline X-9A at the National Synchrotron Light Source of Brookhaven National Laboratories was used for all EXAFS studies, with Si (111) or (220) crystals in unfocused mode [resolution was ≤3 eV (1 eV = 1.6×10^{-19} J)]. Harmonics from the x-ray monochromator were rejected by a mirror. A 13-element energy-resolving germanium detector from Canberra Industries (18) was used to collect the EIAV and peptide data. The germanium detector was run at internal count rates of 40,000 counts per channel per s to minimize dead time losses. A conventional integrating detector (19) with a nickel oxide filter was used to collect the zinc meso-tetraphenylporphyrin (TPP) [4 nitrogens, 2.037 Å average distance (20)], and zinc sulfide [4 sulfurs, 2.346 Å average distance (21)] data. A liquid nitrogen cryostat was used for these experiments and has been described in detail previously; all data were collected at 170 K (22). The ZnS and ZnTPP were studied as solids diluted with aluminum oxide (1:10 by weight) by grinding in a mortar and pestle.

RESULTS AND DISCUSSION

EXAFS data for the EIAV pellet are shown in Fig. 1. The edge jump is consistent with the concentration reported by atomic absorption. The data are manipulated to remove the contribution from the absorption edge and this "background-subtracted" data for the peptide and EIAV are shown in Fig. 2. Data are Fourier transformed (FT) to convert to a radial distribution function, and the virus, peptide, and model compound FT data are shown in Figs. 3 and 4. The FT data are quite instructive, since they show the central metal environment directly. The peptide and virus data are an apparent combination of the nearest-neighbor contributions of the ZnTPP and ZnS models with main peaks intermediate (≈1.8 Å) between the ZnTPP (1.6 Å) and ZnS (2.0 Å) main peaks. The shoulder at 1.2 Å and the peak at 2.4 Å for ZnTPP, virus, and peptide are typical side lobes of the main peak resulting from truncation of a finite data set (23).

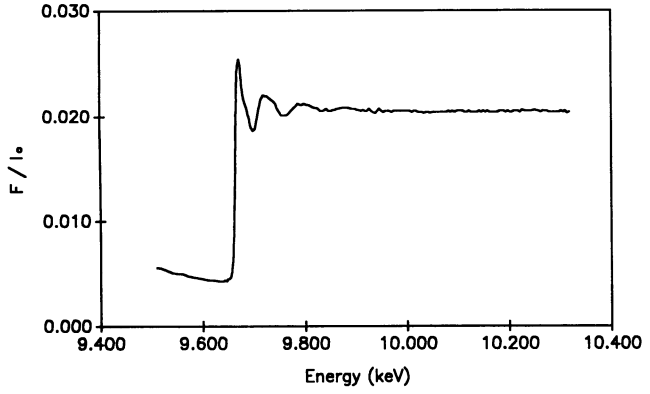

FIG. 1. X-ray fluorescence spectrum of EIAV (1.5 mM in zinc). The spectrum shows reasonable signal-to-noise characteristics and represents total signal averaging of 24 s per point. The x-ray fluorescence divided by a reference scatterer is plotted versus energy. Data were collected in 3-eV increments in the EXAFS region.

The peptide data at greater relative distances from zinc show little structure, while the ZnTPP data clearly show the TPP macrocycle contributions (α carbons at 3.0 Å and β carbons at 3.8 Å) and the ZnS data show the other zinc atoms in the vicinity (3.5 Å). These FT data show only the *relative* radial distances and only suggest a contribution of both sulfur and nitrogen ligands to zinc in the peptide. The histidine of the Cys_3His_1 array in the peptide should be observable, since it is a rigid scatterer; however, no distinct peak above the noise is discernible. By comparison, the FT data of the virus show a strong signal at 3.0 Å. Previous EXAFS studies of the Cys_4 zinc finger from the glucocorticoid receptor show minimal backscattering from the methene carbons of the cysteines (24). This may be due to disorder in the positions of these carbon atoms. Thus, we do not expect a strong signal from these carbons in the virus or peptide. EXAFS studies of the zinc environment of transcription factor IIIA (which has two histidine residues) show a clear higher shell signal (25). The ZnTPP spectrum provides markers close to the expected positions of the histidine higher-shell atoms, since the pyrrole α carbons of the TPP are similar in relative position to the closest histidine carbons. We have separately determined that the peptide structure is less constrained than the corresponding NC protein from HIV-1 because the truncated

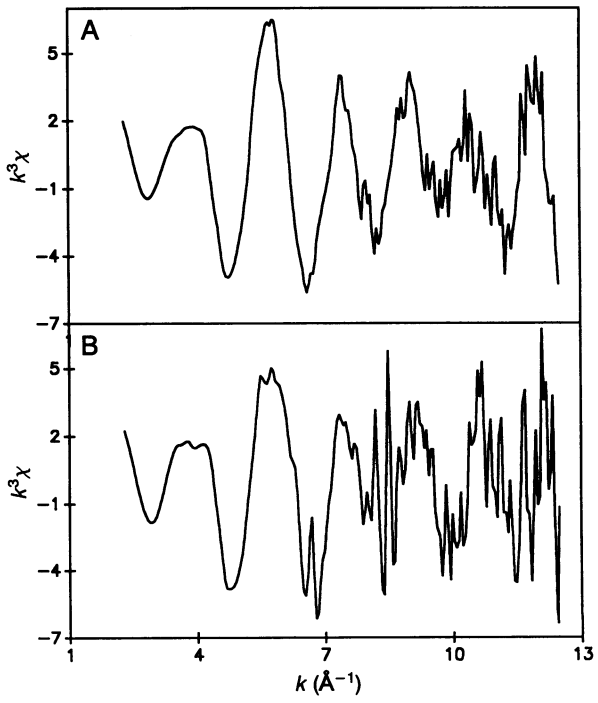

FIG. 2. Wave-vector cube-weighted and background-subtracted χ data of the peptide (*A*) and virus (*B*). The χ data are multiplied by k^3 to enhance the oscillations at high k values, so that the low k values do not dominate the nonlinear-least-squares fitting. k is the momentum of the photoelectron ejected from the central atom: $k = [2m(E - E_0)/h^2]^{1/2}$, in which m is the mass, E is the incident x-ray energy, E_0 is the absorption edge value, and h is Planck's constant. The background removal (or isolated atom subtraction) was accomplished by using B-spline fits across the post-edge region. Windows from 1.5 to 12.5 Å^{-1} were used to generate the FT data of Fig. 4.

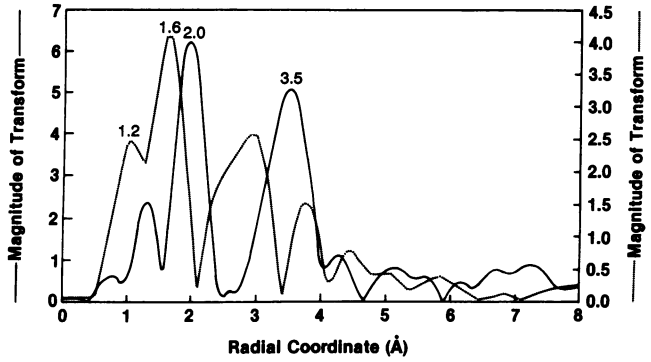

FIG. 3. Fourier transforms of ZnTPP and ZnS χ data. The transform magnitude is plotted versus the relative radial distance from the central atom in Å. The ZnTPP (solid line, left ordinate) shows a main peak from the four coordinated nitrogens at 1.6 Å (with side lobes at 1.2 and 2.4 Å) and TPP macrocycle contributions at 3.0, 3.8, and 4.6 Å. The ZnS (dotted line, right ordinate) shows a main peak from the coordinated sulfur atoms at 2.0 Å and the distant zinc atoms at 3.5 Å. Fourier filter windows from 1.0 to 2.6 Å were applied to this data to provide nitrogen and sulfur contributions for fitting the virus and peptide first shell filtered data. A window from 2.6 to 3.4 Å was applied to the ZnTPP data to provide a carbon contribution to fit the histidine of the virus.

18-residue peptide lacks an apparent hydrogen bonding interaction present in the full-length NC protein (26). Thus, it is not unreasonable to expect a weaker higher-shell signal for this particular peptide compared with an intact virus, if the peptide histidine has a wider distribution of tilt and rotational angles than that in the virus.

The Fourier-filtered data of the peptide and the virus (Fig. 5) show the overall similarities in amplitude and phase of the backscattering from the ligands coordinated to zinc. Fitting these data to models can define the extent to which the zinc sites resemble one another. We measured the distances and Debye–Waller factors of these scatterers by Fourier filtering, back-transforming, and nonlinear least-squares fitting of the peptide and virus data to the models (19, 27–29). The observed truncation artifacts are minimized by matching the window functions of the model compounds and the unknowns. Thus, the model data are reduced, transformed, and back-transformed identically to the unknown data, so that artifacts of the manipulations cancel out. We settled on k-space windows for the virus, peptide, and the two models of 1.5–12.5 $Å^{-1}$ for the forward Fourier transform and r-space windows of 1.0–2.6 Å for the Fourier-filter window. With these windows the data are not extrapolated and sufficient

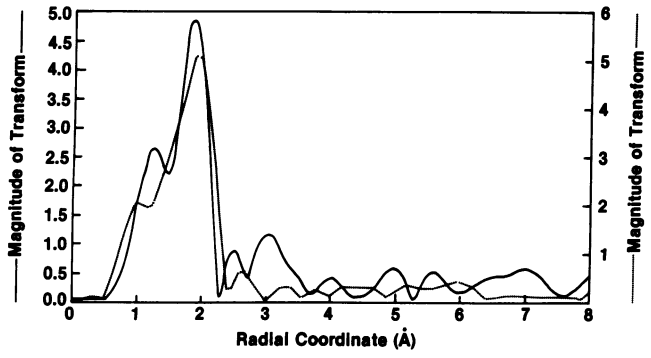

FIG. 4. Fourier transforms of zinc peptide (dotted line, right ordinate) and EIAV (solid line, left ordinate) χ data. The main peaks are both near 1.8 Å, with the virus shifted to slightly shorter distances. Side lobes are seen as a shoulder at 1.2 Å and a peak at 2.4 Å. The virus data have a clear peak at 3.0 Å; this is filtered and fit to the ZnTPP model.

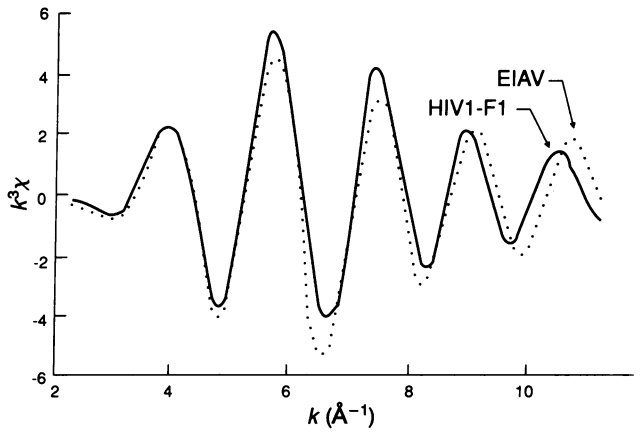

FIG. 5. Fourier-filtered data from EIAV (dotted line) and the HIV-1 F1 peptide (solid line) compared directly. These data result from a window of 1.0–2.6 Å applied to Fig. 4 and back-transformed. The differences in amplitude are very small; the differences in phase correspond to the virus data being 0.05 Å shorter on average than the data from the peptide.

degrees of freedom are available in a two-atom type fit (27), since the data range for fitting is 4–11.5 $Å^{-1}$. The distance errors are estimated by a number of methods described previously (19, 28). Variations in the individual Zn–S distances are not resolved by this procedure; data of this k range are unable to resolve contributions that are separated by ≤0.1 Å (27, 28).

Data analysis with fixed coordination numbers was carried out as described previously, using the University of Washington EXAFS package on a VAX computer (19). We compared several fits with different ratios of sulfur and nitrogen coordination numbers (S:N) held fixed in the fitting procedure (Tables 1 and 2).

We approach the peptide data first, since it has known coordination geometry. In such a case, the different contributions to the data can be resolved by applying fixed coordination numbers in the fitting procedure and searching for possible minima in parameter space (29). These parameters of coordination number are chosen to identify possible candidates for the metal–nitrogen and metal–sulfur distance solutions. For the peptide, if coordination numbers of 3S and 1N are chosen and fixed, using Zn–S models for one atom type and Zn–N models for another, possible distance solutions corresponding to the Zn–histidine nitrogen distance appear opposite the one fixed atom, while the average of the three Zn–S distances appears opposite the fixed contribution of three. In Table 1, the 3:1 S:N fit uses the ZnS model compound to supply a contribution of three sulfur ligands and

Table 1. Nonlinear least-squares fitting of zinc metallopeptide

Ratio of S to N ligands (S:N)	Model	Distance, Å	ΔE_0, eV	$\Delta\sigma^2$, $Å^2$	χ^2
3:1	Zn–S	2.35 ± 0.02	−2	−0.001	3.90
	Zn–N	2.04 ± 0.03	5	−0.005	
3:2	Zn–S	2.36 ± 0.02	−4	−0.002	2.82
	Zn–N	2.06 ± 0.03	5	−0.001	
2:2	Zn–S	2.32 ± 0.02	−5	−0.003	4.90
	Zn–N	2.08 ± 0.03	−2	−0.003	
1:3	Zn–S	2.39 ± 0.03	−6	−0.006	7.6
	Zn–N	2.11 ± 0.04	−5	−0.003	
3:0	Zn–S	2.33 ± 0.05	−2	−0.0005	59.3
4:0	Zn–S	2.35 ± 0.05	−4	0.001	31.2

Coordination numbers are held fixed to resolve the Zn–S and Zn–N contributions to the data. The known coordination numbers provide a good fit to the data, and this set of solutions provides a map of the relationship of parameters for a Cys_3His_1 zinc finger site.

ZnTPP to supply a contribution of one nitrogen ligand. Using the EXAFS equation, we fit this basis set to the unknown data, and we report the distances, Debye–Waller factors, and edge energies for the unknown along with the sum-of-residuals squared (χ^2). The 3:1 S:N fit has a good χ^2, with a Zn–N distance to histidine of 2.04 ± 0.03 Å and the average of the three Zn–S sulfur distances to the cysteines at 2.35 ± 0.02 Å. The Zn–ligand distances observed are reasonable, on the basis of surveys of crystal structure data (30). Thus, with a known peptide coordination, the Zn–ligand distances can be unambiguously defined by EXAFS.

The individual Zn–S distances cannot be distinguished because the resolution of the data, or the ability to distinguish distances differing by less than 0.1 Å, is limited by the data range. However, the Zn–S and Zn–N distances can be easily resolved. Also, N and O are generally not distinguishable. Therefore, an implied Zn–N distance (for example to histidine) would not be distinguishable from a Zn–O distance, to a different ligand. Yet for the peptide, this is not a concern, since previous spectroscopic data restrict the coordination.

In the absence of spectroscopic information that exactly defines the ligand coordination, the 3:1 S:N fit is only one of a family of fits that may be considered possible solutions based *solely* on the Fourier-filtered first-shell EXAFS analysis. In each other case presented in Table 1, we assume a certain combination of coordinating ligands and then find the combination of distances, disorder factors, and edge shifts that give a best fit to the data. Thus, a 3:2 S:N fit is good, while the 2:2 S:N fit has a χ^2 value only slightly higher than the 3:1 S:N fit (meaning it is not significantly different). However, the other fits are poor; 3:0, 4:0, and 1:3 S:N fits have χ^2 values outside a reasonable range. EXAFS alone suggests multiple sulfur ligands and clearly rejects sulfur-only coordination.

Previous investigations of the copper protein stellacyanin illustrated the difficulties in establishing the individual sulfur and nitrogen coordination numbers in cases where both are present and the total coordination number is four or five (31). This is due to the cross-correlation of parameters in the fit, especially the coordination number and the Debye–Waller factor. Notice, in comparing the 3:1 S:N and 3:2 S:N fits for Tables 1 and 2, that the Debye–Waller factors opposite the fixed nitrogen contributions become more positive for the 3:2 S:N fit. The relationship of Debye–Waller factors and amplitudes for the EXAFS equation is such that a more positive Debye–Waller factor tends to reduce the amplitude, while increasing the coordination number has the opposite effect. Therefore, a range of solutions with comparable χ^2 values and Debye–Waller factors shifted less than 0.01 Å^2 from the models is unavoidable (31). The possible results, based on Table 1 alone, imply a 3:1, 3:2, or 2:2 sulfur-to-nitrogen coordination ratio.

However, the analysis of Table 1 provides a detailed map of the fitting solutions for a Cys_3His_1 zinc site. Therefore, this family of fits may represent a fingerprint for the expected family of solutions when such a site is present. We anticipate that any significant deviation from the relationship of fits (relative order of χ^2 and Debye–Waller factors) seen in Table 1 would indicate that 3:1 S:N coordination is inconsistent with an unknown data set. Table 2 shows the family of fitting results for EIAV. The relationships among the family of fits are extraordinarily similar to those found for the peptide in terms of relative χ^2 and $\Delta\sigma^2$ values for the same fixed coordination numbers. The major difference (also seen in Fig. 4) is zinc–ligand distances ≈0.05 Å shorter for the virus. Although EIAV has two cysteine arrays per NC protein, the Debye–Waller factors of Table 2 are reasonable; thus the two *distinct sites* are judged to be exceedingly similar. The first-shell data support a 3:1 S:N coordination based on the similarity of the fitting analysis for the characterized peptide and the virus. Since the N ligand is presumed to be from histidine, the higher-shell contribution of the virus must be consistent with the appropriate carbons of histidine. We filtered and back-transformed the virus and ZnTPP data from 2.6 to 3.4 Å. We derived the average Zn–carbon distances windowed by this filtering by analysis of the ZnTPP structure (20) available in the Cambridge Crystallographic Database (12 carbons at a $1/r^2$ average distance of 3.18 Å). This provided a model for measuring the distances of the higher-shell scatterers present in the virus data. We fit these two filtered data sets to each other with free parameters of N (coordination number), r (distance, Å), $\Delta\sigma^2$ (Debye–Waller factor, Å^2), and ΔE_0 (energy shift). The result was 2 ± 4 atoms at 3.09 ± 0.03 Å with a ΔE_0 of −4.5 eV and a $\Delta\sigma^2$ of 0.006 Å^2, χ^2 = 6.3. The amplitude errors of such a Fourier-filtered higher-shell analysis are typically large, but the distance and disorder factors are typical of histidine coordination (23). The Fourier-filtered higher-shell data of EIAV compared with the simulation are shown in Fig. 6. The fitting result (3.09 Å) is not surprising, in that the α carbon peak of ZnTPP (seen at ≈3.0 Å, actual distance ≈3.07 Å) is observed at the same approximate position as the peak observed in the virus data. Thus, the evidence is strong that the virus site is coordinated by three sulfurs (presumably cysteines) and one histidine ligand.

Table 2. Nonlinear least-squares fitting results of EIAV

Ratio of S to N ligands (S:N)	Model	Distance, Å	ΔE_0, eV	$\Delta\sigma^2$, Å^2	χ^2
3:1	Zn–S	2.30 ± 0.01	4	0.001	1.63
	Zn–N	2.01 ± 0.03	5	−0.001	
3:2	Zn–S	2.30 ± 0.02	2	0.001	1.30
	Zn–N	2.04 ± 0.03	5	0.004	
2:2	Zn–S	2.31 ± 0.02	2	−0.002	2.40
	Zn–N	2.02 ± 0.03	5	0.003	
1:3	Zn–S	2.37 ± 0.02	2	0.005	3.50
	Zn–N	2.09 ± 0.03	5	0.0004	
3:0	Zn–S	2.30 ± 0.03	4	0.004	17.20
4:0	Zn–S	2.28 ± 0.03	6	0.002	6.33

The 3:1 S:N coordination numbers provide a good fit and the relationship of fitting parameters is virtually identical to that of Table 1. The significant difference is the consistently shorter zinc–ligand distance for the virus data.

Previous zinc finger studies by EXAFS have focused on the "classical" (Cys_2His_2) zinc fingers from transcription factor IIIA (25) and the Cys_4 zinc fingers found in the glucocorticoid receptor (24). In the latter case, adequate fits of Fourier-filtered first-shell data were not possible when any contribution from nonsulfur backscatterers was used. Thus,

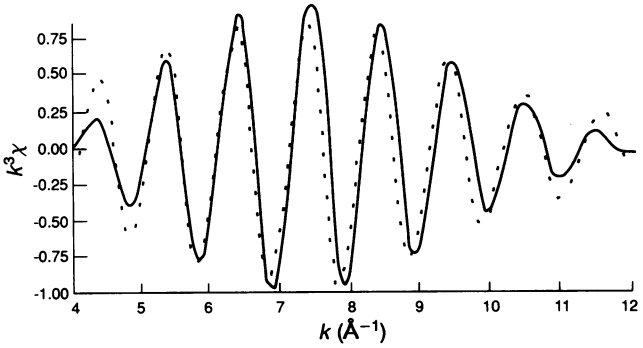

FIG. 6. EIAV data of Fig. 4 windowed from 2.6 to 3.4 Å and back-transformed (solid line). This data set is fit to data from ZnTPP, using an identical window. A minimum is observed where the suggested Zn–carbon average distance is 3.09 Å, consistent with the α carbons of a histidine residue (23, 25). The broken line is the simulated data set based on the ZnTPP model.

the evidence is strong for sulfur-only coordination in the glucocorticoid receptor, especially since only two kinds of zinc site are present. Also, having a single type of backscatterer is a relatively simple EXAFS problem. In the case of EIAV, it is clear that an all-sulfur environment is inadequate to fit the data. However, our Zn–S distances are identical, within the error, to those seen in the glucocorticoid receptor (2.30 Å versus 2.32 Å).

In transcription factor IIIA, there are 7–11 zinc sites. The unfiltered EXAFS data were simulated with two sulfur ligands, two nitrogen ligands, and appropriate higher-shell atoms from the histidines. This resulted in fits where the average Zn–S distances were 2.30 Å and the average Zn–N distances were 2.00 Å. These are virtually identical to our reported distances. The average distance from zinc to the α carbons of histidine was reported at 3.07 Å; our distance is similar at 3.09 Å. Although the existence of low Debye–Waller factors was used as an indication that the 7–11 zinc finger sites were similar, quantitative comparison to other ratios of coordinated ligands was not given. In our study, the analytical problem is simplified by the availability of the peptide model and only two types of zinc site.

Retroviral zinc biochemistry provides a model system wherein metalloprotein structural data critical to understanding retroviral function can be obtained on an intact organism. The zinc present in EIAV is coordinated in a Cys_3His_1 environment. This clearly demonstrates that the role of zinc is to provide a nucleus for folding of the cysteine array into a retroviral type finger structure. EXAFS solutions with less than two sulfurs, or with no nitrogen ligand, are clearly incompatible with the data. The EIAV shows a strong higher-shell signal consistent with histidine carbons. The similarity of the fitting analysis for the zinc peptide model and the virus strongly supports an identical coordination environment. Of further significance is that the metal–ligand distances for the retroviral preparation are shorter than those for the 18-residue peptide. Are these differences in structure due to the truncation of the peptide relative to NC proteins, or does binding of viral RNA influence the structure at zinc? Further experiments with longer peptides complexed with nucleic acids, using both NMR and x-ray methods, are reasonable on the basis of these findings.

This research is supported by grants from the National Institutes of Health and from the Petroleum Research Fund, administered by the American Chemical Society. Michael Grimes and Haleem Issaq assisted in the preparation of virus and atomic absorption spectroscopy. Beamline X-9A at the National Synchrotron Light Source is supported by the National Institutes of Health, the National Science Foundation, and the Department of Energy.

1. Henderson, L. E., Copeland, T. D., Sowder, R. C., Smythers, G. W. & Oroszlan, S. (1981) *J. Biol. Chem.* **256**, 8400–8406.
2. Copeland, T. D., Morgan, M. A. & Oroszlan, S. (1984) *Virology* **133**, 137–145.
3. Green, L. M. & Berg, J. M. (1989) *Proc. Natl. Acad. Sci. USA* **86**, 4047–4051.
4. Berg, J. (1986) *Science* **232**, 485–487.
5. Gorelick, R. J., Henderson, L. E., Hanser, J. P. & Rein, A. (1988) *Proc. Natl. Acad. Sci. USA* **85**, 8420–8424.
6. Meric, C. & Goff, S. P. (1989) *J. Virol.* **63**, 1558–1568.
7. Gorelick, R. J., Nigida, S. M., Bess, J. W., Arthur, L. O., Henderson, L. E. & Rein, A. (1990) *J. Virol.* **64**, 3207–3211.
8. Gorelick, R. J., Nigida, S. M., Arthur, L. O., Henderson, L. E. & Rein, A. (1991) *Advances in Molecular Biology and Targeted Treatment for AIDS*, ed. Kumar, A. (Plenum, New York), pp. 257–272.
9. South, T. L., Kim, B. & Summers, M. F. (1989) *J. Am. Chem. Soc.* **111**, 395–396.
10. Green, L. & Berg, J. M. (1990) *Proc. Natl. Acad. Sci. USA* **87**, 6403–6407.
11. Roberts, W. J., Pan, T., Elliott, J. I., Coleman, J. E. & Williams, K. R. (1989) *Biochemistry* **28**, 10043–10047.
12. Jentoft, J. E., Smith, L. M., Fu, X., Johnson, M. & Leis, J. (1988) *Proc. Natl. Acad. Sci. USA* **85**, 7094–7098.
13. Bess, J. W., Powell, P. J., Issaq, H. J., Schumack, L. J., Grimes, M. K., Henderson, L. E. & Arthur, L. O. (1992) *J. Virol.* **66**, 840–847.
14. Gonda, M. A., Charaman, H. P., Walker, J. L. & Coggins, L. (1978) *Am. J. Vet. Res.* **39**, 431–440.
15. Tajima, M., Nakajima, H. & Ito, Y. (1969) *J. Virol.* **4**, 521–527.
16. Summers, M. F., South, T. L., Kim, B. & Hare, D. R. (1990) *Biochemistry* **29**, 329–340.
17. South, T. L., Blake, P. R., Hare, D. R. & Summers, M. F. (1991) *Biochemistry* **30**, 6342–6349.
18. Cramer, S. P., Tench, O., Yocum, M. & George, G. N. (1988) *Nucl. Instrum. Methods* **A266B**, 586–591.
19. Sagi, I., Wirt, M. D., Chen, E., Frisbie, S. & Chance, M. R. (1990) *J. Am. Chem. Soc.* **112**, 8639–8644.
20. Scheidt, W. R., Mondal, J. U., Eigenbrot, C. W., Adler, A., Radonovich, L. J. & Hoard, J. L. (1986) *Inorg. Chem.* **25**, 795–799.
21. Hückel, W. (1951) *Structural Chemistry of Inorganic Compounds* (Elsevier, New York), Vol. 2, p. 588.
22. Powers, L., Chance, B., Ching, Y. & Angiolillo, P. (1981) *Biophys. J.* **34**, 465–498.
23. Co, M. S., Scott, R. A. & Hodgson, K. O. (1981) *J. Am. Chem. Soc.* **103**, 986–988.
24. Freedman, L. P., Luisi, B. F., Korszun, R., Basavappa, R., Sigler, P. B. & Yamamoto, K. R. (1988) *Nature (London)* **334**, 543–546.
25. Diakun, G. P., Fairall, L. & Klug, A. (1986) *Nature (London)* **324**, 698–699.
26. Summers, M. F., Henderson, L. E., Chance, M. R., Bess, J. W., South, T. L., Blake, P. R., Sagi, I., Perez-Alvarado, G., Sowder, R. C., Hare, D. R. & Arthur, L. O. (1992) *Protein Sci.* **1**, 563–574.
27. Lee, P., Citrin, P., Eisenberger, P. & Kincaid, B. (1981) *Rev. Mod. Phys.* **53**, 769–806.
28. Lytle, F., Sayers, D. & Stern, E. (1989) *Physica B (Amsterdam)* **158**, 701–722.
29. Chance, M. R., Powers, L., Kumar, C. & Chance, B. (1986) *Biochemistry* **25**, 1259–1265.
30. Vedani, A. & Huhta, D. W. (1990) *J. Am. Chem. Soc.* **112**, 4759–4767.
31. Peisach, J., Blumberg, W. H., Powers, L. & Chance, B. (1982) *Biophys. J.* **38**, 277–285.